RAA 2018 Vol. **18** No. **3**, 26(16pp) doi: 10.1088/1674–4527/18/3/26

http://www.raa-journal.org *http://iopscience.iop.org/raa*

***R**esearch in*
***A**stronomy and*
***A**strophysics*

Statefinder diagnostic and constraints on the Palatini $f(R)$ gravity theories

Shu-Lei Cao[1], Song Li[2], Hao-Ran Yu[3] and Tong-Jie Zhang[1,4]

[1] Department of Astronomy, Beijing Normal University, Beijing 100875, China; *tjzhang@bnu.edu.cn*
[2] Department of Physics, Capital Normal University, Beijing 100048, China
[3] Tsung-Dao Lee Institute, Shanghai Jiao Tong University, Shanghai 200240, China
[4] School of Information Management, School of Physics and Electric Information, Shandong Provincial Key Laboratory of Biophysics, Dezhou University, Dezhou 253023, China

Received 2017 October 21; accepted 2017 November 14

Abstract We focus on a series of $f(R)$ gravity theories in Palatini formalism to investigate the probabilities of producing late-time acceleration for the flat Friedmann-Robertson-Walker (FRW) universe. We apply a statefinder diagnostic to these cosmological models for chosen series of parameters to see if they can be distinguished from one another. The diagnostic involves the statefinder pair $\{r, s\}$, where r is derived from the scale factor a and its higher derivatives with respect to the cosmic time t, and s is expressed by r and the deceleration parameter q. In conclusion, we find that although two types of $f(R)$ theories: (i) $f(R) = R + \alpha R^m - \beta R^{-n}$ and (ii) $f(R) = R + \alpha \ln R - \beta$ can lead to late-time acceleration, their evolutionary trajectories in the $r - s$ and $r - q$ planes reveal different evolutionary properties, which certainly justify the merits of the statefinder diagnostic. Additionally, we utilize the observational Hubble parameter data (OHD) to constrain these models of $f(R)$ gravity. As a result, except for $m = n = 1/2$ in case (i), $\alpha = 0$ in case (i) and case (ii) allow the ΛCDM model to exist in the 1σ confidence region. After applying the statefinder diagnostic to the best-fit models, we find that all the best-fit models are capable of going through the deceleration/acceleration transition stage with a late-time acceleration epoch, and all these models turn to the de Sitter point ($\{r, s\} = \{1, 0\}$) in the future. Also, the evolutionary differences between these models are distinct, especially in the $r - s$ plane, which makes the statefinder diagnostic more reliable in discriminating cosmological models.

Key words: dark energy — cosmology: miscellaneous — methods: data analysis

1 INTRODUCTION

Observations of type Ia supernovae (SNeIa) (Perlmutter et al. 1999; Riess et al. 1998) suggest that the universe is currently at an accelerated expansion epoch that is attributed to the dominant component of the universe, dark energy, which not only has a large negative pressure, but also does not cluster as ordinary matters do. In fact, there is no justification for assuming that dark energy resembles known forms of matter or energy, since it has not been detected directly. Up until now, the physical origin of dark energy as well as its nature remains enigmatic.

The simplest model of dark energy is the cosmological constant Λ (Sahni & Starobinsky 2000; Copeland et al. 2006), whose energy density remains constant with time, $\rho_\Lambda = \Lambda/8\pi G$ (natural units $c = \hbar = 1$ are used throughout the paper), and whose equation of state (defined as the ratio of pressure to energy density) remains $w = 1$ as the universe evolves. Unfortunately, the model is burdened with the well known cosmological constant problems, namely the fine-tuning problem: why is the energy of the vacuum so much smaller than we estimate it should be? It also faces the cosmic coincidence problem: why is the dark energy density approximately equal to the matter density today? These

problems have led many researchers to try different approaches for the dark energy issue. Furthermore, recent analysis of SNIa data indicates that time dependent dark energy gives a better fit than the cosmological constant. Instead of assuming the equation of state w is a constant, some authors investigate the dynamical scenarios of dark energy. The most popular model among them is dubbed quintessence (Ratra & Peebles 1988; Peebles & Ratra 1988; Ostriker & Steinhardt 1995), which invokes an evolving scalar field ϕ with a self-interaction potential $V(\phi)$ minimally coupled to gravity. Recently, Zhao et al. (2017) found that the dynamical dark energy model is preferred at a 3.5σ significance level based on the latest observations. Moreover, other scalar-field dark energy models have been studied, including phantom (Caldwell et al. 2003; Singh et al. 2003), tachyon (Sen 2002; Padmanabhan 2002), quintom (Guo et al. 2005; Feng et al. 2005) and ghost condensates (Arkani-Hamed et al. 2004; Piazza & Tsujikawa 2004). Also, there are other candidates, for example, Chaplygin gas which attempts to unify dark energy and dark matter (Bento et al. 2002, 2004), braneworld models which interpret the acceleration through the fact that general relativity (GR) is formulated in five dimensions instead of the usual four (Csáki et al. 2000), backreaction models that consider dark energy as a backreaction effect of inhomogeneities on the average expansion of the universe (Buchert 2000; Räsänen 2004; Kolb et al. 2006) and so forth.

On the other hand, more and more researchers have made a great deal of effort to consider modifying Einstein's GR in order to interpret accelerated expansion of the universe without the existence of dark energy. As is well known, there are numerous ways to generalize Einstein's theory, in which the most famous alternative to GR is scalar-tensor theory (Brans & Dicke 1961; Wagoner 1970). There are still various proposals, for example, Dvali-Gabadadze-Porrati (DGP) gravity (Dvali et al. 2000; Deffayet et al. 2002) and $f(R)$ gravity (Kerner 1982; Allemandi et al. 2004). The so-called $f(R)$ gravity is a straightforward generalization of the Einstein-Hilbert action by including nonlinear terms in the scalar curvature. It has been shown that some of these additional terms can give accelerating expansion without dark energy (Carroll et al. 2004).

Generally, in deriving the Einstein field equations there are two different variational principles that one can apply to the Einstein-Hilbert action, viz., the metric and the Palatini approach. The choice of the variational principle is usually referred to as a formalism, so one can use the metric formalism and the Palatini formalism. In the metric formalism, the connection is assumed to be the Christoffel symbol defined in terms of the metric and the action is only varied with respect to the metric. While in the latter, the metric and the connection are both treated as independent variables, and one varies the action with respect to both of them. In fact, for an action which is linear with Ricci scalar R, both approaches are equivalent, and the theory reduces to GR. However, when the action includes nonlinear functions of R, different field equations are derived from the two methods.

It was pointed out by Dolgov and Kawasaki that the fourth order equations in the metric formalism suffer a serious instability problem (Dolgov & Kawasaki 2003; Soussa & Woodard 2004; Woodard 2007), however, the Palatini formalism provides second order field equations, which are free from the instability problem mentioned above (Meng & Wang 2003, 2004). Additionally, for the metric approach, the models of type $f(R) = R - \beta/R^n$ are incompatible with solar system experiments (Chiba 2003) and the fact that they have the correct Newtonian limit seemed to be a controversial issue (Sotiriou 2006b,a). Another important point is that these models cannot produce a standard matter-dominated era followed by an accelerating expansion (Amendola et al. 2007a,b). However, for the Palatini approach the models satisfy the solar system tests but also have the correct Newtonian limit (Sotiriou 2006a). Furthermore, it has been shown that the above type can produce the sequence of radiation-dominated, matter-dominated and late accelerating phases in Fay et al. (2007). Thus, as already mentioned, the Palatini approach seems appealing though some issues are controversial, such as the instability problems (Sotiriou 2006a; Cembranos 2006). Anyhow, we concentrate on the Palatini formalism.

In addition, since more and more cosmological models have been proposed, the problem of discriminating different models is emergent. In order to tackle this issue, a sensitive and robust diagnosis for dark energy models is required. It is well known that the equation of state w is able to discriminate some of the dark energy models, for example, the cosmological constant Λ with $w = -1$, the quintessence with $w > -1$, the phantom with $w < -1$ and so on. However, for some geometrical models arising from modifications to the gravitational part of Einstein's theory, the equation of state w no longer plays the essential role and its ambit becomes ambiguous. Therefore,

a new diagnosis is requisite to distinguish all classes of cosmological models. In order to achieve this goal, Sahni et al. (2003) introduce the statefinder pair $\{r, s\}$, where r is derived from the scale factor a and its higher derivatives with respect to cosmic time t, and s is expressed by r and the deceleration parameter $q \equiv -a\ddot{a}/\dot{a}^2$. Thus, the statefinder is a "geometrical" diagnostic in the sense that it depends upon the scale factor and hence upon the metric describing spacetime. Based on different cosmological models, distinctions of the evolutionary trajectories in the $r - s$ plane are vivid, which means that the statefinder diagnostic is possibly valid for discriminating different cosmological models. In recent works (Alam et al. 2003; Zhang 2005; Setare et al. 2007; Yi & Zhang 2007), the statefinder diagnostic has been successfully demonstrated to be able to differentiate a series of cosmological models, including the cosmological constant, quintessence, phantom, Chaplygin gas, holographic dark energy, interacting dark energy and so forth.

In this paper, we focus on a flat Friedmann-Robertson-Walker (FRW) universe of the $f(R)$ theory in Palatini formalism and consider a number of $f(R)$ theories recently proposed in the literature. In the meantime, we apply the statefinder diagnostic to these $f(R)$ theories. Two types of $f(R)$ theories: (i) $f(R) = R + \alpha R^m - \beta R^{-n}$ and (ii) $f(R) = R + \alpha \ln R - \beta$ are taken into account. Consequently, we find that the models in the Palatini $f(R)$ gravity can be distinguished from one another, as well as the ΛCDM model. In addition, we employ the observational Hubble parameter data (OHD), which are obtained by the differential galactic age method and the radial Baryon Acoustic Oscillation (BAO) method, to make a combinational constraint. Thereafter, with the best-fit results, we procure the evolutionary trajectories through statefinder diagnostic. Eventually, the results indicate that not only can they demonstrate the possibilities of late-time acceleration, but also they can demonstrate the limpid distinctions between models.

This paper is organized as follows: In Section 2, we briefly review the $f(R)$ gravity in Palatini formalism and study the cosmological dynamical behavior of Palatini $f(R)$ theories. In Section 3, we apply the statefinder diagnostic to a series of $f(R)$ gravity models. In Section 4, we illustrate the results obtained from the observational constraints and apply statefinder diagnosis to the best-fits. Finally, the conclusions and discussions are presented in Section 5.

2 THE PALATINI $F(R)$ GRAVITY AND ITS COSMOLOGICAL DYNAMICS

2.1 A Brief Overview of $f(R)$ Gravity in Palatini Formalism

We firstly review the Palatini formalism from the generalized Einstein-Hilbert action

$$S = \frac{1}{2\kappa}\int d^4x\sqrt{-g}f(R) + S_m(g_{\mu\nu}, \psi), \qquad (1)$$

where $\kappa \equiv 8\pi G$, G is the gravitational constant, g is the determinant of the metric $g_{\mu\nu}$ (Greek indices such as μ, ν run through 0...3 throughout the paper), $f(R)$ is the general function of the generalized Ricci scalar $R \equiv g^{\mu\nu}R_{\mu\nu}(\Gamma^{\lambda}_{\mu\nu})$, and S_m is the matter action which depends only upon the metric $g_{\mu\nu}$ and the matter fields ψ and not upon the independent connection $\Gamma^{\lambda}_{\mu\nu}$ that is differentiated from the Levi-Civita connection $\{^{\lambda}_{\mu\nu}\}$. It should be noted that when $f(R) = R$, GR will come about.

Varying the action with respect to the metric $g_{\mu\nu}$ and the connection $\Gamma^{\lambda}_{\mu\nu}$ respectively yields

$$f'(R)R_{\mu\nu} - \frac{1}{2}f(R)g_{\mu\nu} = \kappa T_{\mu\nu}, \qquad (2)$$

and

$$\overline{\nabla}_{\lambda}(\sqrt{-g}f'(R)g^{\mu\nu}) = 0, \qquad (3)$$

where $f'(R) \equiv df/dR$, $\overline{\nabla}_{\lambda}$ denotes the covariant derivative associated with the independent connection $\Gamma^{\lambda}_{\mu\nu}$ and $T_{\mu\nu}$ is the energy-momentum tensor given by

$$T_{\mu\nu} = \frac{-2}{\sqrt{-g}}\frac{\delta S_m}{\delta g^{\mu\nu}}. \qquad (4)$$

If we consider a perfect fluid case, then $T^{\mu\nu} = (\rho + p)u^{\mu}u^{\nu} + pg^{\mu\nu}$, where ρ, p and u^{μ} denote the energy density, pressure and four-velocity of the fluid, respectively. Note that $T \equiv g^{\mu\nu}T_{\mu\nu} = -\rho + 3p$. Based on Equation (3), we can define a metric conformal to $g_{\mu\nu}$ as

$$h_{\mu\nu} \equiv f'(R)g_{\mu\nu}. \qquad (5)$$

Then, we can deduce the connection $\Gamma^{\lambda}_{\mu\nu}$ in terms of the conformal metric $h_{\mu\nu}$

$$\Gamma^{\lambda}_{\mu\nu} = \frac{1}{2}h^{\lambda\sigma}(\partial_{\mu}h_{\nu\sigma} + \partial_{\nu}h_{\mu\sigma} - \partial_{\sigma}h_{\mu\nu}), \qquad (6)$$

or, equivalently, in regard to $g_{\mu\nu}$

$$\Gamma^{\lambda}_{\mu\nu} = \frac{1}{2f'(R)}g^{\lambda\sigma}[\partial_{\mu}(f'(R)g_{\nu\sigma}) + \partial_{\nu}(f'(R)g_{\mu\sigma}) - \partial_{\sigma}(f'(R)g_{\mu\nu})]. \qquad (7)$$

The corresponding Ricci tensor under the conformal transformation reads

$$R_{\mu\nu} = \partial_\lambda \Gamma^\lambda_{\mu\nu} - \partial_\nu \Gamma^\lambda_{\mu\lambda} + \Gamma^\lambda_{\lambda\sigma}\Gamma^\sigma_{\mu\nu} - \Gamma^\lambda_{\mu\sigma}\Gamma^\sigma_{\lambda\nu}, \quad (8)$$

which can be represented by the Ricci tensor $R_{\mu\nu}(g)$ associated with $g_{\mu\nu}$ as

$$\begin{aligned} R_{\mu\nu} =& R_{\mu\nu}(g) + \frac{3}{2(f'(R))^2}(\nabla_\mu f'(R))(\nabla_\nu f'(R)) \\ & - \frac{1}{f'(R)}(\nabla_\mu\nabla_\nu + \frac{1}{2}g_{\mu\nu}\nabla_\sigma\nabla^\sigma)f'(R), \end{aligned} \quad (9)$$

where ∇_μ is the covariant derivative with respect to the Levi-Civita connection $\{^\lambda_{\mu\nu}\}$ of the metric $g_{\mu\nu}$.

2.2 FRW Cosmology of the Palatini $f(R)$ Gravity and Numerical Results

Since measurements of Cosmic Microwave Background (CMB) suggest that our universe is spatially flat (Halverson et al. 2002; Netterfield et al. 2002) at late times, we start with a flat FRW universe with metric

$$ds^2 = -dt^2 + a^2(t)(dx^2 + dy^2 + dz^2), \quad (10)$$

where $a(t)$ and t are the scale factor and cosmic time, respectively.

According to Equations (2) and (9), the modified Friedmann equation can be derived as

$$\left(H + \frac{\dot{f}'(R)}{2f'(R)}\right)^2 = \frac{\kappa(\rho + 3p) + f(R)}{6f'(R)}, \quad (11)$$

where $H \equiv \dot{a}/a$ is the Hubble parameter, and the dot denotes differentiation with respect to the cosmic time t. In addition, taking the trace of Equation (2) gives

$$f'(R)R - 2f(R) = \kappa T. \quad (12)$$

If we assume that the universe only contains dust-like (pressureless) matter at late times, then $T = -\rho_m$, where ρ_m represents the energy density of matter. Furthermore, combining Equation (12) with the energy conservation equation of matter $\dot{\rho}_m + 3H\rho_m = 0$, we can express $\dot{R}$ as

$$\dot{R} = -\frac{3H\Big[f'(R)R - 2f(R)\Big]}{f''(R)R - f'(R)}, \quad (13)$$

where $f''(R) \equiv d^2f/dR^2$. Substituting Equation (13) into Equation (11), we can obtain

$$H^2 = \frac{1}{6f'}\frac{3f - f'R}{\left[1 - \frac{3f''(f'R-2f)}{2f'(f''R-f')}\right]^2}. \quad (14)$$

Since the redshift z can be expressed through $1 + z = a_0/a$ and conventionally the present scale factor $a_0 = 1$ is chosen (subscript 0 denotes the present time value throughout the paper), we can get the expressions $\rho_m = \rho_{m0}(1 + z)^3$ and $dz/dt = -H(1 + z)$. Therefore, Equations (12) and (13) can be rewritten as

$$f'(R)R - 2f(R) = -3H_0^2\Omega_{m0}(1+z)^3, \quad (15)$$

and

$$\frac{dR}{dz} = -\frac{9H_0^2\Omega_{m0}(1+z)^2}{f''(R)R - f'(R)}, \quad (16)$$

where $\Omega_{m0} \equiv \kappa\rho_{m0}/3H_0^2$. As a result, Equation (14) can also be expressed as

$$\frac{H^2}{H_0^2} = \frac{1}{6f'}\frac{3\Omega_{m0}(1+z)^3 + f/H_0^2}{\left[1 + \frac{9H_0^2\Omega_{m0}(1+z)^3 f'')}{2f'(f''R-f')}\right]^2}. \quad (17)$$

In order to study the cosmological evolution by using Equations (15)–(17), it is prerequisite to obtain the initial conditions: (R_0, H_0, Ω_{m0}). With Equations (15) and (17), choosing units so that $H_0 = 1$ (Amarzguioui et al. 2006), once the explicit expression of $f(R)$ is given, one can solve for R_0 with fixed value of Ω_{m0}. On the other hand, in order to understand the cosmological evolution behavior, it is useful to define the effective equation of state

$$w_{\text{eff}} = -1 + \frac{2}{3}(1+z)\frac{H'}{H}, \quad (18)$$

where $H' \equiv dH/dz$. Since the deceleration parameter q is related as follows

$$q = -1 + (1+z)\frac{H'}{H} = \frac{1}{2}(1 + 3w_{\text{eff}}), \quad (19)$$

one can certainly explore the cosmological dynamics through the evolutions of w_{eff} with different models of Palatini $f(R)$ gravity.

2.2.1 $f(R)$ *theories with power-law terms*

We consider the following general form for $f(R)$

$$f(R) = R + \alpha R^m - \beta R^{-n}, \quad (20)$$

where m and n are real constants with the same sign. Such theories have been investigated to explain the early and late accelerated expansion of our universe (Sotiriou 2006b; Meng & Wang 2004). Note that not all combinations of m and n are in agreement with a flat universe with the early matter dominated era followed by an accelerated expansion at late times. At the early times of matter-dominated era, the universe is better described by

GR in order to avoid confliction with early-time physics such as Big Bang Nucleosynthesis (BBN) and CMB. It implies that the modified Lagrangian should recover the standard GR Lagrangian for large R, and hence it requires $m < 1$ and $n > -1$. Then, we consider two specific types of theories in this regime.

(i) The $\alpha = 0$ case In this case, the form of $f(R)$ reads

$$f(R) = R - \beta R^{-n}. \tag{21}$$

Based on Equations (16)–(18), by adopting $H_0 = 1$ and $\Omega_{m0} = 0.27$, we can obtain the evolutions of the scalar curvature R and the effective equation of state $w_{\rm eff}$ that are shown in Figure 1. Note that the special case of $(\beta, n) = (4.38, 0)$ corresponds to the ΛCDM model. From Figure 1, one can easily see that for any choice of n ($n > -1$), the curvature R and the effective equation of state $w_{\rm eff}$ decrease with the evolution of the universe. Moreover, the smaller n is, the faster R decreases, and the larger the present values of $w_{\rm eff}$ are. Also, the expansion of the universe can turn from a decelerated phase into an accelerated phase, and the universe approaches de Sitter phase in the future. Interestingly, one can see from Figure 1 that there is an intermediate convergence zone where the redshift is around 1.2, and the evolutionary trajectories are upsidedown through the convergence zone. From the perspective of mathematics, the convergence zone must be caused by the slope change of the effective equation of state $w_{\rm eff}$, since they all have the same constraints but for different expressions of $f(R)$. From Equation (20), one can certainly see that the value of $f(R)$ is sensitive as the power n varies, including its derivatives with respect to R. The variances embodied in Figure 1 are clear: As the redshift grows, at first, the slopes of the curves are slowly increased, and then they become steady, and at last, the slopes slowly decrease to zero in the future. Therefore, the different dropping rates of $w_{\rm eff}$ lead to the convergence. Also, it is worth noticing that in the $n = 0.4$ case, the slope changes from negative to positive.

(ii) The $m = n = -1/2$ case

In this case, Equation (20) becomes

$$f(R) = R + \alpha R^{1/2} - \beta R^{-1/2}. \tag{22}$$

Figure 2 is plotted by going through the same procedure as the above case. One can ascertain that the curvature R and the effective equation of state $w_{\rm eff}$ decrease with evolution for different choices of β. Furthermore, the smaller β results in the faster decrease of R, and larger $w_{\rm eff}$ at the present time. It is also obvious that the universe evolves from deceleration to acceleration, and enters de Sitter acceleration in the future.

2.2.2 $f(R)$ theories with a logarithmic term

Finally we exploit $f(R)$ theories of the type

$$f(R) = R + \alpha \ln R - \beta, \tag{23}$$

which have been studied in Nojiri & Odintsov (2004); Meng & Wang (2004), and it has been claimed that such theories have a well-defined Newtonian limit (Nojiri & Odintsov 2004). Note that the asymptotic behavior $\lim_{R\to\infty} f(R) \to R$ is obtained for any choice of α and β, and thus, the arbitrary α and β can satisfy the assumption that the universe can be described by GR at the early times. However, not all combinations of α and β can explain a late-time accelerated expansion of the universe. Therefore, for the sake of compatibility with the observational constraints obtained in Section 4, we select a series of values of β which can well represent the evolvement of the universe from an early-time deceleration to a late-time acceleration (see also Fig. 3).

Substituting Equation (23) into Equations (16)–(18), with $H_0 = 1$ and $\Omega_{m0} = 0.27$, the evolvements of the curvature R and the effective equation of state $w_{\rm eff}$ with respect to the redshift z are illustrated in Figure 3. Consequently, R and $w_{\rm eff}$ decrease with the evolution of the universe for the set of β. Also, the larger β gets, the slower the decrease of R and the smaller the $w_{\rm eff}$ at the present time appear to be. Similarly to the results of the above types of theories, the universe evolves from deceleration to acceleration, and gets close to a de Sitter universe in the future.

3 STATEFINDER DIAGNOSTIC FOR THE PALATINI $F(R)$ GRAVITY

In this section, we pay attention to the statefinder diagnosis. As is well known, two famous geometrical variables characterizing the expansion history of the universe are the Hubble parameter H representing the expansion rate of the universe and the deceleration parameter $q \equiv -a\ddot{a}/\dot{a}^2$ characterizing the rate of acceleration/deceleration of the expanding universe. Obviously, they only depend on the scale factor a and its first and second derivatives in terms of t, i.e., $\dot{a}$ and $\ddot{a}$. However,

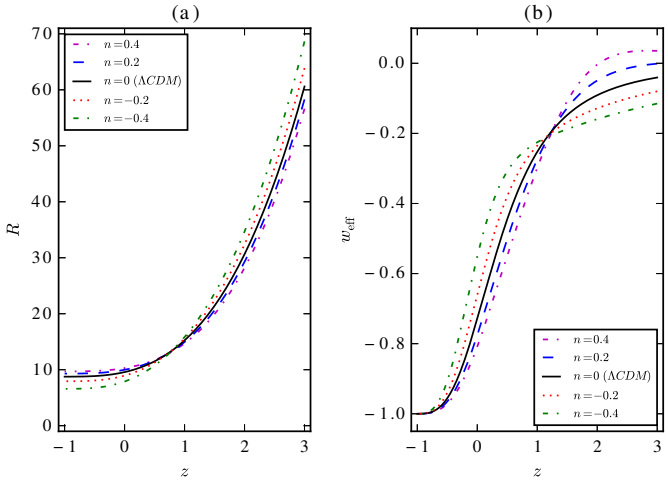

Fig. 1 The evolutions of the scalar curvature R and the effective equation of state $w_{\rm eff}$ versus redshift z for $f(R) = R - \beta R^{-n}$. Different values of n are chosen, along with $H_0 = 1$ and $\Omega_{m0} = 0.27$.

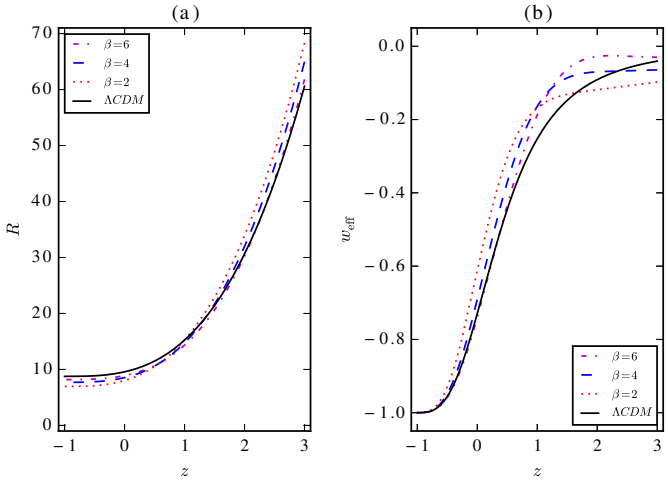

Fig. 2 Same as Fig. 1, except for theories of type $f(R) = R + \alpha R^{1/2} - \beta R^{-1/2}$. Different values of β are chosen, along with $H_0 = 1$ and $\Omega_{m0} = 0.27$.

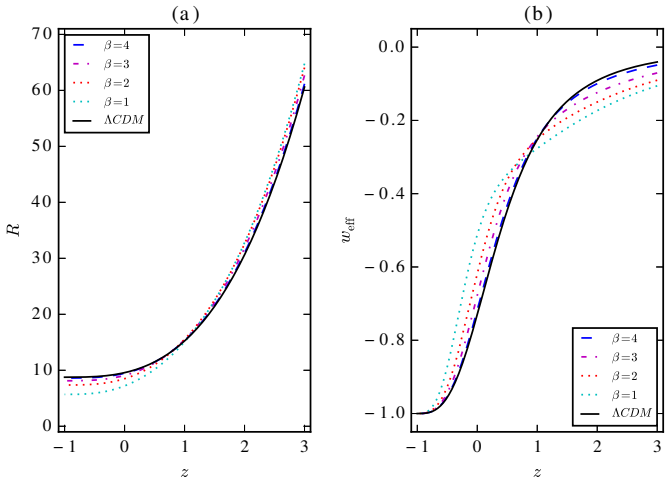

Fig. 3 Same as Fig. 1, except for theories of type $f(R) = R + \alpha \ln R - \beta$.

with the increasing amount of cosmological models and the remarkable increase in the accuracies of cosmological observational data, these two parameters are no longer sensitive enough for distinguishing different models, which can be revealed from the fact that many cosmological models correspond to the same current value of q. As a result, the so-called statefinder diagnosis was introduced in order to discriminate more and more cosmological models involving dark energy. It can be constructed using both the second and third derivatives of the scale factor a.

In addition to H and q, two new parameters are defined as the statefinder pair $\{r, s\}$

$$r \equiv \frac{\dddot{a}}{aH^3}, \qquad s \equiv \frac{r-1}{3(q-1/2)}. \tag{24}$$

Since different cosmological models exhibit distinct evolutionary trajectories in the $r-s$ plane, the statefinder diagnostic is probably a fine tool to distinguish cosmological models. The remarkable property is that $\{r, s\} = \{1, 0\}$ corresponds to the ΛCDM model. So, one can clearly identify the "distance" from a given cosmological model to the ΛCDM model in the $r-s$ plane, such as the quintessence, phantom, Chaplygin gas, holographic dark energy and interacting dark energy models, which have been studied in the literatures (Alam et al. 2003; Zhang 2005; Setare et al. 2007; Yi & Zhang 2007). In particular, the current values of parameters s and r in these diagrams can provide a useful way to measure the "distance" from a given model to the ΛCDM model.

According to Equation (19), the statefinder pair $\{r, s\}$ can be rewritten as

$$r = 1 - 2(1+z)\frac{H'}{H} + (1+z)^2\left(\frac{H'^2}{H^2} + \frac{H''}{H}\right), \tag{25}$$

$$s = \frac{-2(1+z)H'/H + (1+z)^2(H'^2/H^2 + H''/H)}{3[-3/2 + (1+z)H'/H]}, \tag{26}$$

where $H'' \equiv d^2H/dz^2$.

In what follows, we apply the statefinder diagnostic to the $f(R)$ theories mentioned in Section 2. However, due to the fact that a singularity comes when the denominator of s tends to zero (i.e., $q = 0.5$ case), which can be seen from Figure 5(b), the values of parameters we deliberately select in such theories are not all the same as those in the previous section. Comparing Figure 5 with Figure 4(c), one can palpably find that not all combinations of α and β are suitable for statefinder diagnosis. Next, we will show that $r-s$ planes display the distinct evolutionary trajectories for these Palatini $f(R)$ theories, and hence one can discriminate various types of Palatini $f(R)$ theories from one another, not to mention other dark energy models.

Table 1 The currently available OHD dataset. Method I is the differential galactic age method, and II represents the radial BAO method. $H(z)$ is in units of $\mathrm{km\,s^{-1}\,Mpc^{-1}}$ here.

z	$H(z)$	Method	Reference
0.0708	69.0 ± 19.68	I	Zhang et al. (2014)
0.09	69.0 ± 12.0	I	Jimenez et al. (2003)
0.12	68.6 ± 26.2	I	Zhang et al. (2014)
0.17	83.0 ± 8.0	I	Simon et al. (2005)
0.179	75.0 ± 4.0	I	Moresco et al. (2012)
0.199	75.0 ± 5.0	I	Moresco et al. (2012)
0.20	72.9 ± 29.6	I	Zhang et al. (2014)
0.240	79.69 ± 2.65	II	Gaztañaga et al. (2009)
0.27	77.0 ± 14.0	I	Simon et al. (2005)
0.28	88.8 ± 36.6	I	Zhang et al. (2014)
0.35	84.4 ± 7.0	II	Xu et al. (2013)
0.352	83.0 ± 14.0	I	Moresco et al. (2012)
0.3802	83.0 ± 13.5	I	Moresco et al. (2016)
0.4	95 ± 17.0	I	Simon et al. (2005)
0.4004	77.0 ± 10.2	I	Moresco et al. (2016)
0.4247	87.1 ± 11.2	I	Moresco et al. (2016)
0.43	86.45 ± 3.68	II	Gaztañaga et al. (2009)
0.44	82.6 ± 7.8	II	Blake et al. (2012)
0.4497	92.8 ± 12.9	I	Moresco et al. (2016)
0.4783	80.9 ± 9.0	I	Moresco et al. (2016)
0.48	97.0 ± 62.0	I	Stern et al. (2010)
0.57	92.4 ± 4.5	II	Samushia et al. (2013)
0.593	104.0 ± 13.0	I	Moresco et al. (2012)
0.6	87.9 ± 6.1	II	Blake et al. (2012)
0.68	92.0 ± 8.0	I	Moresco et al. (2012)
0.73	97.3 ± 7.0	II	Blake et al. (2012)
0.781	105.0 ± 12.0	I	Moresco et al. (2012)
0.875	125.0 ± 17.0	I	Moresco et al. (2012)
0.88	90.0 ± 40.0	I	Stern et al. (2010)
0.9	117.0 ± 23.0	I	Simon et al. (2005)
1.037	154.0 ± 20.0	I	Moresco et al. (2012)
1.3	168.0 ± 17.0	I	Simon et al. (2005)
1.363	160.0 ± 33.6	I	Moresco (2015)
1.43	177.0 ± 18.0	I	Simon et al. (2005)
1.53	140.0 ± 14.0	I	Simon et al. (2005)
1.75	202.0 ± 40.0	I	Simon et al. (2005)
1.965	186.5 ± 50.4	I	Moresco (2015)
2.34	222.0 ± 7.0	II	Delubac et al. (2015)

Figure 4 demonstrates the evolutions of r and s with respect to redshift z for $f(R)$ theories mentioned above. It can be shown that different features are exhibited as follows:

(1) For the model $f(R) = R - \beta R^{-n}$ (see also Fig. 4(a)), the curves stay at one side of the ΛCDM

line ($r = 1$ and $s = 0$). Specifically, for the $n > 0$ case, the evolutionary curves lie in the region $r > 1, s < 0$, and for the $n < 0$ case, inversely, they remain in the region $r < 1, s > 0$. Moreover, the trajectories of evolution are all first moving away from the ΛCDM line and then towards it. This could evidently be revealed from $r - s$ planes as shown in Figure 6(a). In addition, the larger the absolute values of n become, the further the traces of evolvement move from the ΛCDM line. Eventually, they both tend to evolve like a ΛCDM universe (de Sitter point, i.e., $\{r, s\} = \{1, 0\}$, or $\{q, r\} = \{-1, 1\}$) in the future.

(2) As for the theories of type $f(R) = R + \alpha R^{1/2} - \beta R^{-1/2}$ in Figure 4(b), we can easily find that for any choices of β, the evolutionary curves cross the ΛCDM line sooner or later, and the larger β gets, the bigger the fluctuations of r and s turn. Also, they all will come to an end like the ΛCDM universe in the future.

(3) The models of type $f(R) = R + \alpha \ln R - \beta$ explored in Figure 4 are all the cases for which α and β have opposite sign (note that only for the $\beta > 0$ case), and in comparison with Figure 5(a) where $\alpha, \beta > 0$ holds, one can realize that evolutions of r depend on the sign of α and β. In the former case, r lies in the region $r < 1$ and also $s > 0$. It is worth mentioning that the "distance" between the evolutionary trajectories and the ΛCDM line grows smaller along with larger values of β. In the latter case, inversely, r lies in the region $r > 1$, and the larger β is, the farther r moves away from the $r = 1$ line. However, both cases turn towards the ΛCDM case in the future.

Anyhow, it is evidently seen from the above features that the trajectories of evolutions vary from different choices of parameters and from model to model. Finally, $r - s$ and $r - q$ planes are plotted in Figure 6. Observing the $r - s$ plane is clearer than just looking at the separate evolutions of r and s, especially when it comes to comparing between cosmological models. After all, this aspect is more palpable for $r - s$ planes with distinct evolutionary trajectories and explicit evolutionary directions to tell the differences. $r - s$ and $r - q$ planes significantly exhibit deviations between the Palatini $f(R)$ theories, and also show that the deceleration/acceleration transition occurs in these models. Therefore, the statefinder diagnostic is a fair way to differentiate various cosmological models.

4 CONSTRAINTS WITH OHD

In order to determine if these $f(R)$ models are compatible with cosmological observations, here we intend to constrain the parameters in the above types of $f(R)$ models with OHD. The currently available OHD dataset is listed in Table 1. With this dataset, we can adopt these $f(R)$ theories in Equation (17), and for the goodness of fit we employ the standard χ^2 minimization, defined by

$$\chi^2 = \sum_i \frac{[H_{\rm th}(z_i|\mathbf{p}) - H_{\rm obs}(z_i)]^2}{\sigma^2(z_i)}, \qquad (27)$$

where $H_{\rm th}(z_i|\mathbf{p})$ is the theoretical Hubble parameter at redshift z_i given by Equation (17), and $\mathbf{p}$ depends on the $f(R)$ models; $H_{\rm obs}(z_i)$ are the OHD, and $\sigma(z_i)$ is the uncertainty of each $H_{\rm obs}(z_i)$. Note that the covariance matrix of data is not necessarily diagonal, as discussed in Yu et al. (2013), and if not, the case will become complicated and should be treated by means of the method mentioned by Yu et al. (2013). Here we assume that each measurement in $\{H_{\rm obs}(z_i)\}$ is independent.

In what follows we will proceed to constrain the models studied in the previous section. When calculating χ^2, we first exploit $H_0 = 1$ in Equations (15)–(17), and then multiply the resulting $H_{\rm th}(z_i)$ by iterated values of H_0. Subsequently, we marginalize the parameters to plot contour figures. Meanwhile, with the best-fits of each model, we apply the statefinder diagnostic to them.

4.1 Theories of the Type $f(R) = R - \beta R^{-n}$

In this context, the set of parameters is selected with $\mathbf{p} = (H_0, \Omega_{m0}, n)$. Figure 7 shows the constraints in the 1σ, 2σ and 3σ confidence regions, in which contour plots showing two out of three parameters are presented by marginalizing the third parameter. The best-fit values of $\mathbf{p}$ are $H_0 = 70\,{\rm km\,s^{-1}\,Mpc^{-1}}$, $\Omega_{m0} = 0.24$, and $n = -0.11$, along with the corresponding value of $\beta = 3.65$. In the combined analysis of Amarzguioui et al. (2006), the best-fit model is found to be $\beta = 3.6$ and $n = -0.09$, which is consistent with our best fits. After marginalizing over H_0, Ω_{m0} and n, the 1σ constraint values are ($\Omega_{m0} = 0.24^{+0.06}_{-0.13}$, $n = -0.11^{+0.49}_{-0.58}$), ($H_0 = 70^{+3.6}_{-4.5}\,{\rm km\,s^{-1}\ Mpc^{-1}}$, $n = -0.09^{+0.47}_{-0.60}$) and ($\Omega_{m0} = 0.25^{+0.055}_{-0.084}$, $H_0 = 70^{+4.3}_{-3.7}\,{\rm km\ s^{-1}\,Mpc^{-1}}$), respectively. Note that the ΛCDM model lies in the 1σ

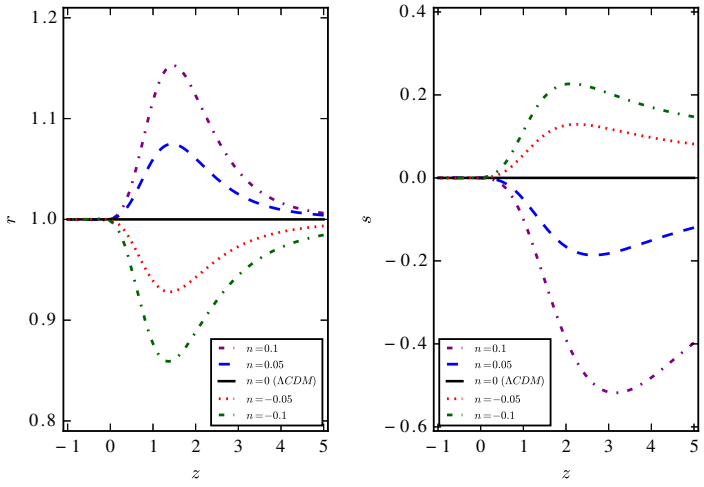

(a)

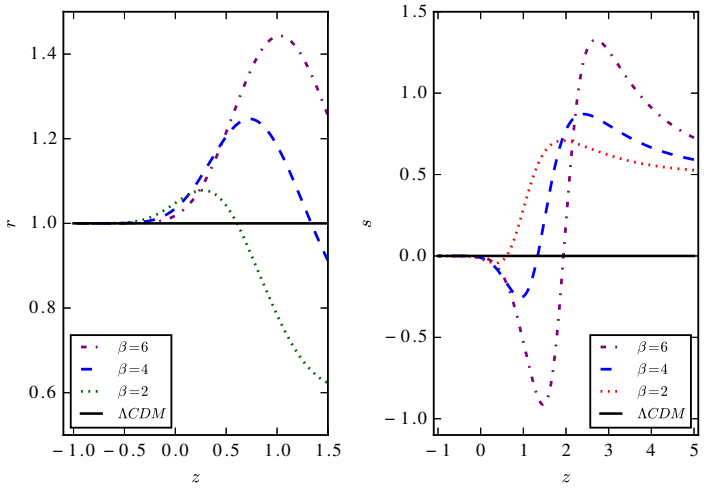

(b)

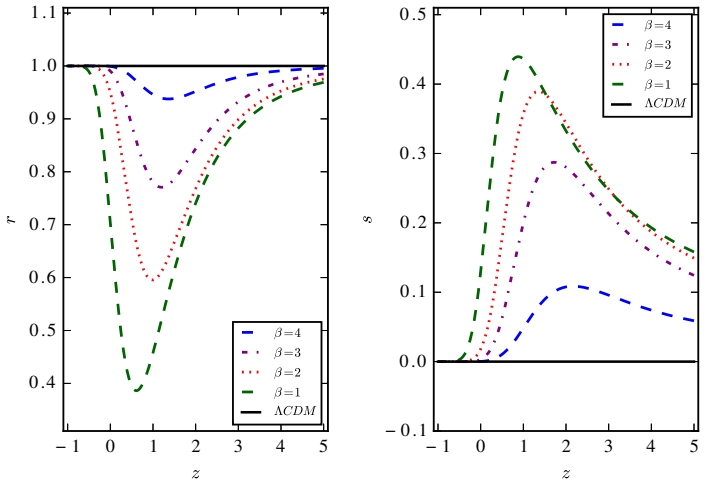

(c)

Fig. 4 Evolutions of $r(z)$ and $s(z)$ for the theories of type $f(R) = R - \beta R^{-n}$ (a), $f(R) = R + \alpha R^{1/2} - \beta R^{-1/2}$ (b) and $f(R) = R + \alpha \ln R - \beta$ (c) with $H_0 = 1$ and $\Omega_{m0} = 0.27$.

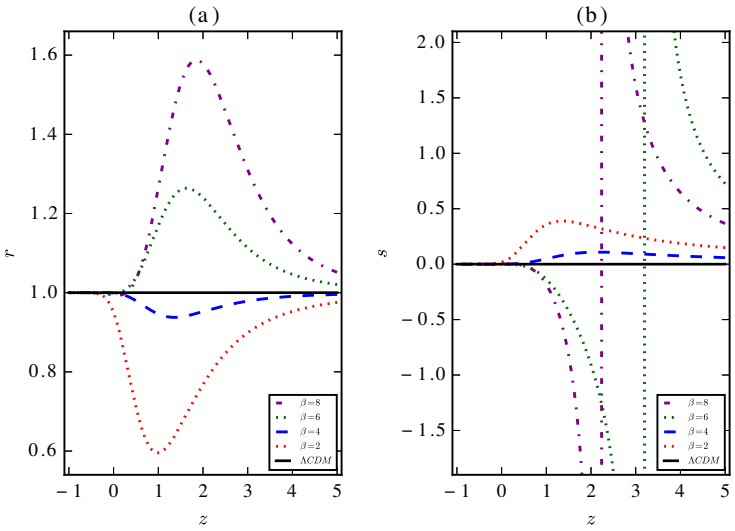

Fig. 5 Same as Fig. 4(c), but for different values of β. Note that the $\beta = 6$ and $\beta = 8$ cases indicate that at times of q around 0.5, s tends to infinity as expected.

confidence level, which corresponds to $\Omega_{m0} = 0.27$ and $n = 0$, marked by a cross in Figure 7.

Since we have the best-fit model of this type, the statefinder diagnostic can be exploited to study its real evolutionary process. As shown in Figure 10, the evolutionary trajectories are indeed compatible with the features described in the previous section for the $n < 0$ case (see also Fig. 6(a)). Evidently, one can find the best-fit model of this type is capable of producing late-time acceleration of the universe and includes the deceleration/acceleration transition stage.

4.2 Theories of the Type $f(R) = R + \alpha R^{1/2} - \beta R^{-1/2}$

In this circumstance, by choosing $\mathbf{p} = (H_0, \Omega_{m0}, \beta)$, we plot the contour figures with the same methods as the previous model in Figure 8. The best-fits of $\mathbf{p}$ are $H_0 = 70\,\mathrm{km\,s^{-1}\,Mpc^{-1}}$, $\Omega_{m0} = 0.18$ and $\beta = 2.1$ associated with $\alpha = -1.53$. By marginalizing over H_0, Ω_{m0} and β separately, we obtain the corresponding 1σ constraints of ($\Omega_{m0} = 0.18^{+0.073}_{-0.039}$, $\beta = 2.2^{+6.60}_{-2.72}$), ($H_0 = 70^{+3.96}_{-4.34}\,\mathrm{km\,s^{-1}\,Mpc^{-1}}$, $\beta = 2.6^{+7.23}_{-3.12}$) and ($\Omega_{m0} = 0.19^{+0.082}_{-0.045}$, $H_0 = 71^{+3.28}_{-4.64}\,\mathrm{km\,s^{-1}\,Mpc^{-1}}$), respectively. This shows an example where the two nonlinear terms of Equation (20) are comparable and necessary to produce the acceleration at late times as Fay et al. (2007) stated. However, our best fits vary from them in the $m = n = 1/2$ case, which may be caused by the different set of parameters being constrained.

In Figure 10, $r - s$ and $r - q$ planes indicate that they fit the characteristics explored in Section 3, and the trajectories of evolvement clearly differ from the other two types of $f(R)$ theories in Palatini formalism. Also, the best-fit model of this type is able to evolve from decelerated expansion to the late-time acceleration of the universe.

4.3 Theories of the Type $f(R) = R + \alpha \ln R - \beta$

In this situation, we set $\mathbf{p}$ to be $(H_0, \Omega_{m0}, \alpha)$. Same as the above methods, the confidence regions are demonstrated in Figure 9, where the best-fit constraints are $H_0 = 70\,\mathrm{km\,s^{-1}\,Mpc^{-1}}$, $\Omega_{m0} = 0.24$ and $\alpha = -0.48$ coupled with $\beta = 3.58$. Consequently, they are not compatible with the best-fit model of Fay et al. (2007) which corresponds to $\alpha = 0.11$ and $\beta = 4.62$, and excludes the $\beta = 0$ case. Although our constraints include the $\beta = 0$ case (when α is around –2.3) in the 2σ region, it means that the assertion made by Fay et al. (2007), that the $\ln R$ term alone cannot drive the late-time acceleration without a cosmological constant, is not tenable, let alone the fact that the ΛCDM model ($\alpha = 0$ and $\Omega_{m0} = 0.27$, marked in Fig. 9) is well contained in the 1σ region. The marginalized 1σ constraints are ($\Omega_{m0} = 0.24^{+0.076}_{-0.050}$, $\alpha = -0.48^{+2.67}_{-1.26}$), ($H_0 = 70^{+3.7}_{-4.6}\,\mathrm{km\,s^{-1}\,Mpc^{-1}}$, $\alpha = -0.3^{+2.80}_{-1.44}$) and ($\Omega_{m0} = 0.25^{+0.082}_{-0.055}$, $H_0 = 71^{+4.0}_{-3.8}\,\mathrm{km\,s^{-1}\,Mpc^{-1}}$)

As shown in Figure 10, as a common feature of the type $f(R) = R - \beta R^{-n}$ and the type $f(R) =$

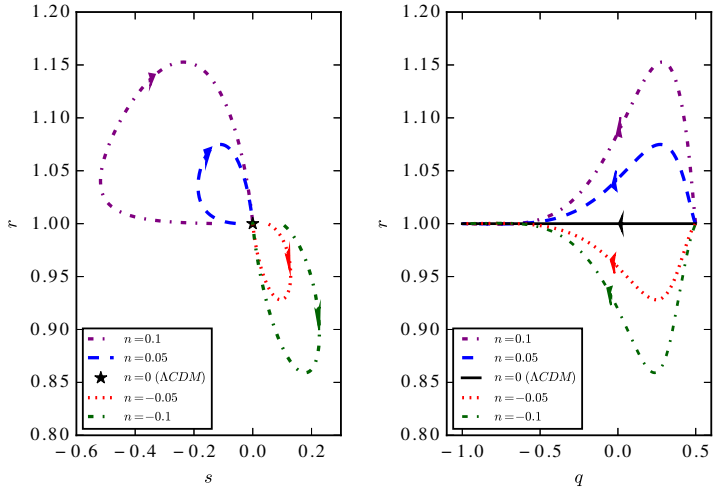

(a)

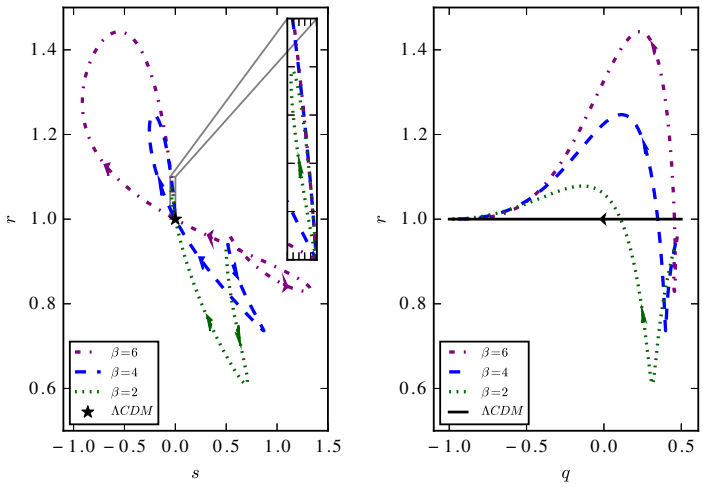

(b)

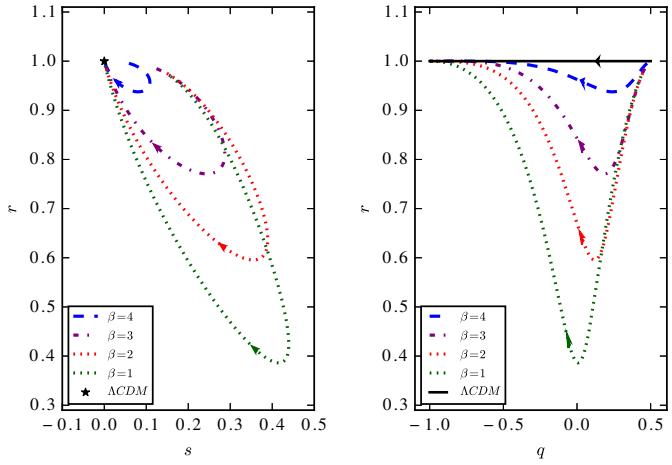

(c)

Fig. 6 Statefinder diagnostic $r-s$ and $r-q$ planes for the theories of type $f(R) = R-\beta R^{-n}$ (a), $f(R) = R+\alpha R^{1/2}-\beta R^{-1/2}$ (b) and $f(R) = R+\alpha \ln R-\beta$ (c) with $H_0 = 1$ and $\Omega_{m0} = 0.27$.

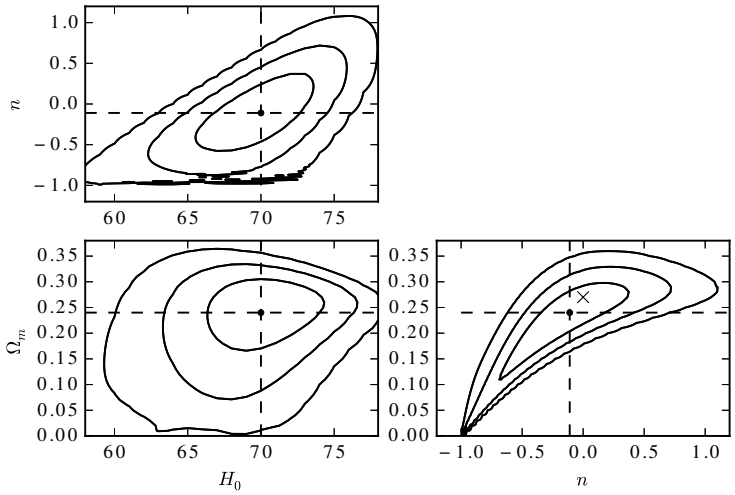

Fig. 7 1σ, 2σ and 3σ confidence regions of the theory $f(R) = R - \beta R^{-n}$ constrained by OHD. The dashed lines and the dots represent the best-fit values of $H_0 = 70\,\mathrm{km\,s^{-1}\,Mpc^{-1}}$, $\Omega_{m0} = 0.24$ and $n = -0.11$. The cross mark represents the ΛCDM model.

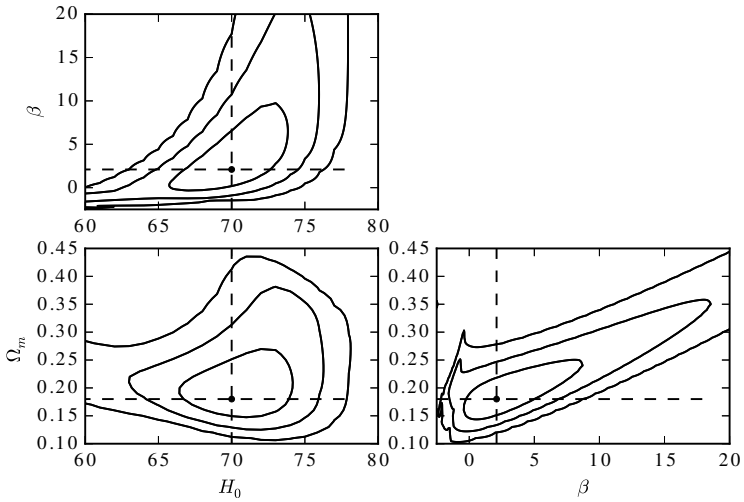

Fig. 8 Same as Fig. 7, but for the theory $f(R) = R + \alpha R^{1/2} - \beta R^{-1/2}$. The dashed lines and dots show the best-fit values of $H_0 = 70\,\mathrm{km\,s^{-1}\,Mpc^{-1}}$, $\Omega_{m0} = 0.18$ and $\beta = 2.1$.

$R + \alpha R^{1/2} - \beta R^{-1/2}$ that we missed in Section 3, the evolutionary trajectories of the best-fit models are almost indistinguishable in the $r - q$ plane, but still distinct in the $r - s$ plane. Therefore, this characteristic further favors the statefinder pair $\{r, s\}$ in the direction of discriminating different cosmological models. Also, the $r - q$ plane shows that the best-fit model of this type can explain the transition of phase from decelerated expansion to the late-time acceleration of the universe.

5 CONCLUSIONS AND DISCUSSION

In previous sections, we have systematically studied the cosmological dynamics of a series of types of $f(R)$ theories within the Palatini approach and applied the statefinder diagnostic to these models, and then placed observational constraints on the parameters of the models.

First, we find that different features of evolutionary trails of the Ricci curvature R and the effective equation

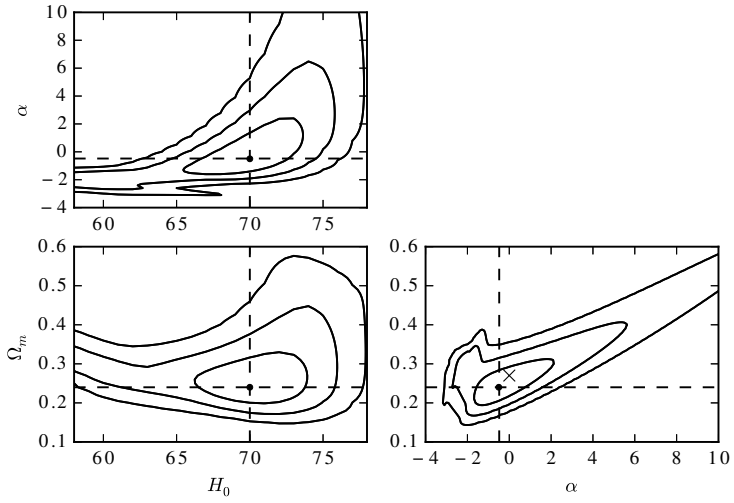

Fig. 9 Same as Fig. 7, but for the theory $f(R) = R + \alpha \ln R - \beta$. The dashed lines and the dots exhibit the best-fit values of $H_0 = 70\,\mathrm{km\,s^{-1}\,Mpc^{-1}}$, $\Omega_{m0} = 0.24$ and $\alpha = -0.48$. The cross mark represents the ΛCDM model.

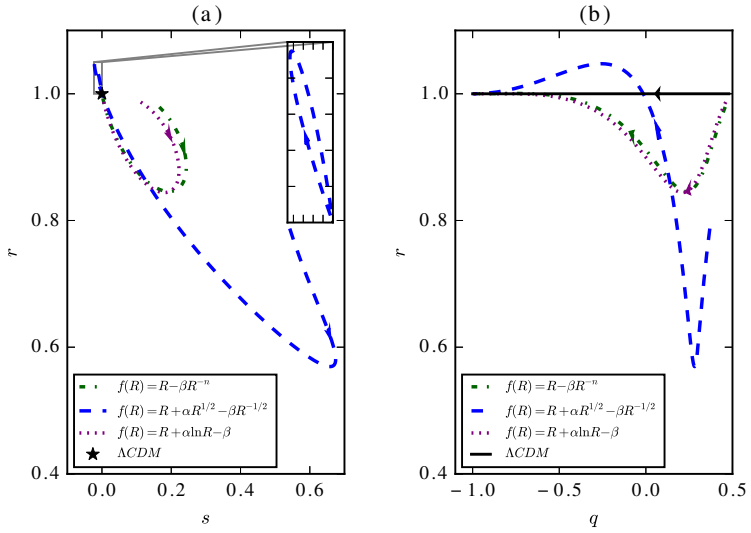

Fig. 10 Statefinder pairs $r - s$ and $r - q$ planes for the best-fit models of the Palatini $f(R)$ theories of type $f(R) = R - \beta R^{-n}$, $f(R) = R + \alpha R^{1/2} - \beta R^{-1/2}$ and $f(R) = R + \alpha \ln R - \beta$.

of state $w_{\rm eff}$ with respect to redshift z are revealed. For all the models of Palatini $f(R)$ theory, the values of order index n ($n > -1$) for R in Equation (21), the parameter β in Equation (22) and the parameter β in Equation (23) all have negative correlations with the decreased rate of R, and positive correlations with the fluctuations of $w_{\rm eff}$.

Second, since more and more theories have been proposed to account for the late-time accelerated expansion of the universe, the well-known parameters, such as the Hubble parameter H, the deceleration parameter q and equation of state w, are not enough to discriminate these models. In particular, for the case of modified gravity theories such as string/M-theory, extended scalar-tensor models and braneworld models of dark energy, the equation of state w is not a fundamental physical entity. The more general and sensitive diagnosis known as statefinder diagnostic emerges as required. However, it makes one wonder if this diagnosis can stand the trial at all times. Therefore we employ it in the $f(R)$ theories of types described by Equations (21), (22) and (23), to see if it can still hold well for the sake of discrimination. Eventually, one can draw conclusions that the trajectories

of evolutions vary from model to model and with a different set of values for the given parameters, and also the $r-s$ and $r-q$ planes further exhibit clear differences among the models. As a result, the $f(R)$ theories with chosen series of parameters not only display distinct trajectories of evolvement, but also present evident deceleration/acceleration transition along with late-time acceleration and tendency towards the ΛCDM model in the future. Thus, the statefinder diagnostic holds for this literature as an efficient way to distinguish between cosmological models. We believe that further explorations into its validity will be made in future researches for more and more cosmological models, and even if it somewhat fails, more advanced diagnosis would be proposed. In some sense, now that $\dot{a}$, $\ddot{a}$ and $\dddot{a}$ are involved, the fourth and even fifth order derivatives of the scale factor a are more probable to be included to enhance the accuracy of the diagnostic.

Third, we exploit OHD to obtain observational constraints on the models in Equations (21), (22) and (23). On one hand, the best-fits of Equation (21) are compatible with the combined constraints of Amarzguioui et al. (2006), but not consistent with the constraints of Fay et al. (2007). Also, the goodness of fit is separated from Fay et al. (2007) for both models described by Equations (22) and (23). On the other hand, for the first model in Equation (21), the ΛCDM model lies in the 1σ confidence region, as well as the type given by Equation (23). The second model, Equation (22), shows an example where the two nonlinear terms of (20) are comparable and necessary to produce the acceleration at late times. As for the third model in Equation (23), the constraints include the $\beta=0$ case in the 2σ confidence region, which means that the $\ln R$ term alone can possibly drive the late-time acceleration without a cosmological constant.

Ultimately, we employ the statefinder diagnostic in the three best-fit models. As a consequence, for one thing, we find that the evolutionary trajectories have the same properties as described in Section 3. For another thing, it is worth noticing the common features between best-fit models of Equations (22) and (23). On the $r-q$ plane, one can almost not discriminate their trails, but considering the $r-s$ plane as a complement, obviously, the differences between them are certain. This further admits the merits of the statefinder pair $\{r,s\}$. In addition, all the best-fit models of the Palatini $f(R)$ theory have the same properties as follows: (i) They both carry out an earlier-time deceleration and late-time acceleration phase in the matter-dominated universe; (ii) They both tend to turn into ΛCDM cosmology in the future. Notice that in the paper we only consider the flat late-time matter-dominated FRW universe, which is perfectly suitable for OHD for the low redshift range of $0.0708<z<2.34$.

Acknowledgements This work was supported by the National Natural Science Foundation of China (NSFC, Grant Nos. 11573006, 11528306 and 11347163), the Fundamental Research Funds for the Central Universities, the Special Program for Applied Research on Super Computation of the NSFC-Guangdong Joint Fund (the second phase) and the Science and Technology Program Foundation of the Beijing Municipal Commission of Education of China (Grant No. KM201410028003).

Appendix A: RELEVANT DERIVATIVES

In what follows, we give some derivatives in terms of the generalized Ricci curvature R and the redshift z, which can facilitate plotting the statefinder diagnostic.

According to Equation (15), we define parameter A as follows

$$\begin{aligned} A &\equiv \left[1-\frac{3f''(f'R-2f)}{2f'(f''r-f')}\right]^2 \\ &= \left[1+\frac{9f''\Omega_{m0}H_0^2(1+z)^3}{2f'(f''r-f')}\right]^2, \end{aligned} \tag{A.1}$$

and then the Hubble parameter H becomes

$$H=\sqrt{\frac{3f-f'R}{6f'A}}=\sqrt{\frac{3\Omega_{m0}H_0^2(1+z)^3+f}{6f'A}}. \tag{A.2}$$

The first derivative of A in terms of R reads

$$\begin{aligned} A'\equiv\frac{dA}{dR} =& -3\sqrt{A}\Big\{\frac{f'R-2f}{f''R-f'}\Big[\frac{f'''}{f'}-\frac{f''^2}{f'^2} \\ &-\frac{f''f'''R}{f'(f''R-f')}\Big]+\frac{f''}{f'}\Big\}. \end{aligned} \tag{A.3}$$

The second derivative of A is written as

$$\begin{aligned} A''\equiv&\frac{d^2A}{dR^2}=\frac{A'^2}{2A}-3\sqrt{A}\Big\{\Big(\frac{f''''}{f'}-\frac{f'R-2f}{f''R-f'}\frac{3f''f'''}{f'^2} \\ &+\frac{2f'''^3}{f'^3}\Big)+2\Big(\frac{f'''}{f'}-\frac{f''^2}{f'^2}\Big)\Big[1-\frac{f'''R(f'R-2f)}{(f''R-f')^2}\Big] \\ &+\frac{f''}{f'(f''R-f')}\Big[\frac{2f'''^2R^2(f'R-2f)}{(f''R-f')^2} \\ &-\frac{(f'''+f''''R)(f'R-2f)}{f''R-f'}\Big]-f'''R\Big\}. \end{aligned} \tag{A.4}$$

The first derivative of R with respect to redshift z is shown in Equation (16), and the first derivative of H in terms of R is given as

$$\frac{dH}{dR} = \frac{1}{2HA}\Big[\frac{1}{3} + \frac{A'}{2A}\Big(\frac{R}{3} - \frac{f}{f'}\Big) - \frac{ff''}{2f'^2}\Big]. \quad \text{(A.5)}$$

Thus H' relates to dH/dR as follows

$$H' = \frac{dH}{dR}\frac{dR}{dz} = -\frac{dH}{dR}\frac{9\Omega_{m0}H_0^2(1+z)^2}{f''R - f'}. \quad \text{(A.6)}$$

The second derivative of H with respect to R is expressed as

$$\begin{aligned}\frac{d^2H}{dR^2} =& -\frac{(dH/dR)^2}{H} + \frac{1}{2HA}\Big\{\frac{A'}{A}\Big[\frac{A'}{A}\Big(\frac{f}{f'} - \frac{R}{3}\Big) \\ &+ \frac{ff''}{f'^2} - \frac{2}{3}\Big] - \frac{1}{2}\Big[\frac{f''}{f'} + \frac{f}{f'} \\ &+ \frac{f}{f'}\Big(\frac{A''}{A} + \frac{f'''}{f'}\Big)\Big] + \frac{ff''^2}{f'^3} + \frac{A''R}{6A}\Big\},\end{aligned} \quad \text{(A.7)}$$

which corresponds to H'' as follows

$$H'' = \frac{dH}{dR}\frac{d^2R}{dz^2} + \frac{d^2H}{dR^2}\left(\frac{dR}{dz}\right)^2, \quad \text{(A.8)}$$

where the second derivative of R relating to z is

$$\frac{d^2R}{dz^2} = \frac{dR}{dz}\left(\frac{2}{1+z} - \frac{f'''R}{f''R - f'}\frac{dR}{dz}\right). \quad \text{(A.9)}$$

References

Alam, U., Sahni, V., Deep Saini, T., & Starobinsky, A. A. 2003, MNRAS, 344, 1057

Allemandi, G., Borowiec, A., & Francaviglia, M. 2004, Phys. Rev. D, 70, 103503

Amarzguioui, M., Elgarøy, Ø., Mota, D. F., & Multamäki, T. 2006, A&A, 454, 707

Amendola, L., Gannouji, R., Polarski, D., & Tsujikawa, S. 2007a, Phys. Rev. D, 75, 083504

Amendola, L., Polarski, D., & Tsujikawa, S. 2007b, Physical Review Letters, 98, 131302

Arkani-Hamed, N., Creminelli, P., Mukohyama, S., & Zaldarriaga, M. 2004, J. Cosmol. Astropart. Phys., 4, 001

Bento, M. C., Bertolami, O., & Sen, A. A. 2002, Phys. Rev. D, 66, 043507

Bento, M. C., Bertolami, O., & Sen, A. A. 2004, Phys. Rev. D, 70, 083519

Blake, C., Brough, S., Colless, M., et al. 2012, MNRAS, 425, 405

Brans, C., & Dicke, R. H. 1961, Physical Review, 124, 925

Buchert, T. 2000, General Relativity and Gravitation, 32, 105

Caldwell, R. R., Kamionkowski, M., & Weinberg, N. N. 2003, Physical Review Letters, 91, 071301

Carroll, S. M., Duvvuri, V., Trodden, M., & Turner, M. S. 2004, Phys. Rev. D, 70, 043528

Cembranos, J. A. R. 2006, Phys. Rev. D, 73, 064029

Chiba, T. 2003, Physics Letters B, 575, 1

Copeland, E. J., Sami, M., & Tsujikawa, S. 2006, International Journal of Modern Physics D, 15, 1753

Csáki, C., Graesser, M., Randall, L., & Terning, J. 2000, Phys. Rev. D, 62, 045015

Deffayet, C., Dvali, G., & Gabadadze, G. 2002, Phys. Rev. D, 65, 044023

Delubac, T., Bautista, J. E., Busca, N. G., et al. 2015, A&A, 574, A59

Dolgov, A. D., & Kawasaki, M. 2003, Physics Letters B, 573, 1

Dvali, G., Gabadadze, G., & Porrati, M. 2000, Physics Letters B, 485, 208

Fay, S., Tavakol, R., & Tsujikawa, S. 2007, Phys. Rev. D, 75, 063509

Feng, B., Wang, X., & Zhang, X. 2005, Physics Letters B, 607, 35

Gaztañaga, E., Cabré, A., & Hui, L. 2009, MNRAS, 399, 1663

Guo, Z.-K., Piao, Y.-S., Zhang, X., & Zhang, Y.-Z. 2005, Physics Letters B, 608, 177

Halverson, N. W., Leitch, E. M., Pryke, C., et al. 2002, ApJ, 568, 38

Jimenez, R., Verde, L., Treu, T., & Stern, D. 2003, ApJ, 593, 622

Kerner, R. 1982, General Relativity and Gravitation, 14, 453

Kolb, E. W., Matarrese, S., & Riotto, A. 2006, New Journal of Physics, 8, 322

Meng, X. H., & Wang, P. 2003, Classical and Quantum Gravity, 20, 4949

Meng, X.-H., & Wang, P. 2004, Physics Letters B, 584, 1

Moresco, M., Verde, L., Pozzetti, L., Jimenez, R., & Cimatti, A. 2012, J. Cosmol. Astropart. Phys., 7, 053

Moresco, M. 2015, MNRAS, 450, L16

Moresco, M., Pozzetti, L., Cimatti, A., et al. 2016, J. Cosmol. Astropart. Phys., 5, 014

Netterfield, C. B., Ade, P. A. R., Bock, J. J., et al. 2002, ApJ, 571, 604

Nojiri, S., & Odintsov, S. D. 2004, General Relativity and Gravitation, 36, 1765

Ostriker, J. P., & Steinhardt, P. J. 1995, Nature, 377, 600

Padmanabhan, T. 2002, Phys. Rev. D, 66, 021301

Peebles, P. J. E., & Ratra, B. 1988, ApJ, 325, L17

Perlmutter, S., Aldering, G., Goldhaber, G., et al. 1999, ApJ, 517, 565

Piazza, F., & Tsujikawa, S. 2004, J. Cosmol. Astropart. Phys., 7, 004

Räsänen, S. 2004, J. Cosmol. Astropart. Phys., 2, 003
Ratra, B., & Peebles, P. J. E. 1988, Phys. Rev. D, 37, 3406
Riess, A. G., Filippenko, A. V., Challis, P., et al. 1998, AJ, 116, 1009
Sahni, V., Saini, T. D., Starobinsky, A. A., & Alam, U. 2003, Soviet Journal of Experimental and Theoretical Physics Letters, 77, 201
Sahni, V., & Starobinsky, A. 2000, International Journal of Modern Physics D, 9, 373
Samushia, L., Reid, B. A., White, M., et al. 2013, MNRAS, 429, 1514
Sen, A. 2002, Journal of High Energy Physics, 7, 065
Setare, M. R., Zhang, J., & Zhang, X. 2007, J. Cosmol. Astropart. Phys., 3, 007
Simon, J., Verde, L., & Jimenez, R. 2005, Phys. Rev. D, 71, 123001
Singh, P., Sami, M., & Dadhich, N. 2003, Phys. Rev. D, 68, 023522
Sotiriou, T. P. 2006a, General Relativity and Gravitation, 38, 1407
Sotiriou, T. P. 2006b, Phys. Rev. D, 73, 063515
Soussa, M. E., & Woodard, R. P. 2004, General Relativity and Gravitation, 36, 855
Stern, D., Jimenez, R., Verde, L., Kamionkowski, M., & Stanford, S. A. 2010, J. Cosmol. Astropart. Phys., 2, 008
Wagoner, R. V. 1970, Phys. Rev. D, 1, 3209
Woodard, R. 2007, in Lecture Notes in Physics, 720, The Invisible Universe: Dark Matter and Dark Energy, ed. L. Papantonopoulos, 403 (Berlin: Springer Verlag)
Xu, X., Cuesta, A. J., Padmanabhan, N., Eisenstein, D. J., & McBride, C. K. 2013, MNRAS, 431, 2834
Yi, Z.-L., & Zhang, T.-J. 2007, Phys. Rev. D, 75, 083515
Yu, H.-R., Yuan, S., & Zhang, T.-J. 2013, Phys. Rev. D, 88, 103528
Zhang, C., Zhang, H., Yuan, S., et al. 2014, RAA (Research in Astronomy and Astrophysics), 14, 1221
Zhang, X. 2005, International Journal of Modern Physics D, 14, 1597
Zhao, G.-B., Raveri, M., Pogosian, L., et al. 2017, Nature Astronomy, 1, 627